# Resonant states of a double-barrier junction

S. E. Shafranjuk*,† and J. B. Ketterson‡
*Department of Physics and Astronomy, Northwestern University, Evanston Illinois 60208, USA*
(Received 22 February 2005; revised manuscript received 7 April 2005; published 8 July 2005)

We study resonant properties of an SIS′IS junction with quantized Andreev bound states (ABSs); here S, S′ and I denote a superconductor, a superconductor with a smaller energy gap, and an insulating barrier, respectively. Using the quasiclassical approach we compute the local electron density of states, spatial extent of the quantized states and inelastic electron-phonon recombination rate versus junction transparency, nonmagnetic impurity concentration, and the thickness of the middle layer. We find that the local electron density of states in a low-transparency limit has sharp peaks at the ABS level positions while the inelastic electron-phonon recombination time, $\tau_{e\text{-}p}(\varepsilon)$, associated with an ABS level $E_0$ is a sharp function of energy variable $\varepsilon$ and diverges at $\varepsilon=E_0$.

DOI: 10.1103/PhysRevB.72.024509 PACS number(s): 74.50.+r, 73.40.Gk

## I. INTRODUCTION

Quantized states in superconducting quantum wells have been extensively studied both theoretically[1–15] and experimentally.[10,16–21] Up to now the quantized states (referred also as to Andreev bound states or ABSs) were experimentally observed in only a few systems. Scanning tunneling spectroscopy measurements provide evidence for ABS levels in (i) the normal core of an Abrikosov vortex[16] and (ii) normal wires embedded in a superconducting matrix.[17] Multiple Andreev reflection (MAR) features[22–24] have been observed in the current-voltage characteristics of nanojunctions with superconducting leads.[25] Recently an experimental observation of ABS levels was reported[10,18–21] in double barrier SIS′IS junctions.

An SIS′IS junction is shown schematically in Fig. 1(a); here S is a superconducting electrode, I is an insulating barrier, and S′ is a superconductor with an energy gap, $\Delta'$, which is less than $\Delta$, the energy gap in S. Quantized states are formed in the SIS′IS junction with the associated wave function centered on the S′ electrode (where $\Delta' \ll \Delta$ or $\Delta'=0$). The Andreev bound states (ABSs) result from the interference between incident electrons and reflected holes at the SIS′ and S′IS interfaces; the resulting resonant levels, $E_n$, produce sharp peaks in the local electron density of states, $\mathcal{N}(\varepsilon)$, at energies $\varepsilon=E_n$. According to Refs. 2 and 7, the quantization associated with these states is responsible for a *phase-coherent transfer of Josephson supercurrent* across the SIS′IS junction; i.e., the ABSs are then responsible for the Josephson supercurrent itself. An advantage of the SIS′IS junction, as compared to vortices or embedded wires, is that the direction along which the motion is quantized coincides with the measurement current, which allows the injection of supercurrent and quasiparticles directly into the ABS level, which enhances the sensitivity of the measurements. The multilayered superconducting junctions allow exploitation of the Nb-Al technology (where Nb serves as S, Al as S′, and the barrier I is formed with $Al_xO_y$) which yields "clean" layers and high-quality barriers.[10,18–21] In addition the quantum wells in such systems may have various profiles, depending on the thickness of the middle electrode and on the transparency of the insulating barriers. Another benefit of the SIS′IS junction is that the ABS position and width can be controlled by bias supercurrents applied through the junction electrodes in various ways.[21]

Despite significant theoretical progress,[1–10,12–15] the experiments[18–21] raise new questions about the physical properties of the ABS. The barrier transparency $D$ in the multilayered junctions[18–21] is typically low, $10^{-4}-10^{-5}$; therefore only a small fraction of incident electrons are engaged in the Andreev reflection processes at an S′IS interface while the majority of the processes involve ordinary reflections, raising questions about the mechanism of ABS formation in such low-transparency junctions.[18–21] Since the ABSs are formed due to interference between the incident electron and reflected hole waves, one expects that the most favorable resonance conditions are realized in "clean" multilayers with near-perfect interfaces, and at temperatures $T \ll \Delta$. The elastic electron scattering from interface roughness and atomic impurities make the electron and hole trajectories effectively longer. In such "dirty" junctions, an electron (or hole) experiences many collisions prior to each Andreev reflection event; a large number of different trajectories then contribute to the ABS resonance condition. In the "dirty" limit ($\Delta\tau_i \ll 1$, where $\tau_i$ is the elastic collision time) the resonance condition is not clearly defined, and one expects a broadening and ultimately a disappearance of the ABS levels. Precisely how the electron-impurity (and electron-

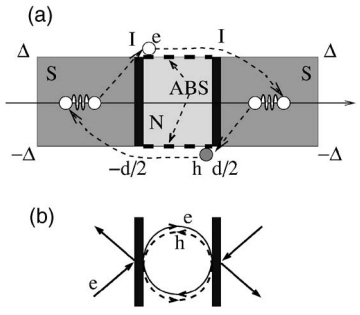


FIG. 1. (a) The double-barrier junction (DBJ) having the SIS′IS structure. (b) The simplest classical trajectories in SIS′IS.

 

phonon) collisions affect the formation of ABS is not well understood. In addition, if the angle of incidence of the electron is finite, the resonance condition is also modified, because the contributing electron-hole trajectories become effectively longer than for normal incidence. Thus the contribution of finite-angle trajectories serves as another source of broadening the ABS resonance.

In this paper we study steady-state properties of quantized states in multilayered junctions. In particular we examine how the quantized states are affected by the interface barriers, by the finite-angle reflection, and by electron-impurity and electron-phonon scattering. The paper is organized as follows. In Sec. II we briefly discuss the concept of Andreev bound states and formulate the quasiclassical equations for envelope functions. In Sec. III we introduce boundary conditions[26,27] and implement the quasiclassical method to formulate a model for Andreev bound states in an SIS′IS junction. We obtain an analytical solution for electron and hole wave functions on classical trajectories and compute the quasiclassical retarded Green function in the junction. In Sec. IV we compute the local electron density of states of a double-barrier Josephson junction and study how the formation of quantized states in the S′ layer depends on the junction transparency and geometry, on the electron-impurity elastic scattering, and on finite-angle electron-hole reflection. In particular, we examine the spatial extend of the ABS. In Sec. V we compute the inelastic electron-phonon recombination rate from an ABS level. Our conclusions are presented in Sec. VI.

## II. QUANTIZED STATES IN DOUBLE BARRIER JUNCTIONS

The standing waves caused by Andreev reflection in an SIS′IS junction result in quantized ABSs. The underlying mechanism is as follows [see Fig. 1(a)]. A Cooper pair in the left S layer can dissociate into a lone electron in S and an electron traveling to the right in the S′ layer. On penetration into the right S electrode, this electron enters the superfluid condensate, but to conserve charge a hole, $h$, is simultaneously created; momentum conservation requires that the hole momentum be opposite to that of the incident electron $e$. The hole (which has a negative energy $-\Delta$) enters and propagates in the middle S′ layer via the negative energy ABS; on encountering and penetrating the left electrode it annihilates the remaining electron of the original Cooper pair. Since the duration time $\tau_{CP}$ of the whole process is $\tau_{CP} \leqslant \hbar/(2\Delta)$, from the quantum mechanical point of view all the parts of the round trip happen simultaneously. In this way a Cooper pair can be transferred from the left S electrode, through two interface barriers and the middle S′ layer, into the right S electrode. In the absence of the supercurrent an equal number of processes occur in the reverse direction. Such processes are to be expected in a superconductor, since the number of Cooper pairs fluctuates. The entire process is shown schematically in Fig. 1(b) where the solid lines correspond to electrons and the dotted lines to holes.

On closer examination the above scenario presents a paradox: since the transparency of the insulating barriers is low (typically $10^{-4}$) we expect the probability for Andreev reflection to be small. If, however, the width of the S′ layer is equal to an integer number of half wavelengths of the envelope of the quasiclassical wave function, a peculiar cooperative coupling occurs between the Cooper pairs in the two S layers and the standing waves in the S′ layer. The energies, $E_n$, at which this condition occurs are the Andreev bound states, and the signature of their presence is sharp peaks in the density of states, $\mathcal{N}(\varepsilon)$, at these energies.

From this discussion we see that Andreev bound states differ greatly from a conventional electron (or hole) (Breit-Wigner) resonant state which results from large barrier heights with reflection coefficients that approach unity (and are essentially energy independent). The resulting amplitude of the quasi-bound state is large only *between* the confining barriers. On the other hand, resonant electron-hole Andreev states in the presence of high barriers (ordinarily leading to small reflection coefficients) require a cooperative behavior of all three media; the resulting bound state amplitude is then large both inside *and* outside the quantum well defined by the barrier. If the middle layer thickness $d \simeq \xi_S$, there are only two ABS levels inside the S′ layer which are positioned at $E_0 \simeq \pm\Delta$, as shown in Fig. 1(a).

In the presence of a supercurrent there is an imbalance in the number of Cooper pairs transferred across the two barriers. This process is coherent because the phase is preserved during the whole transmission process. However, the magnitude of the electric current depends on the phase difference between the two S electrodes in a more complicated way than for the conventional Josephson current through an SIS junction.

Analytic solutions for the ABS have only been obtained for the SS′S and ScS cases (where c denotes a constriction);[28] SIS′IS junctions have only been treated numerically (see Refs. 10 and 20 and references therein). However, to clarify the overall behavior it is instructive to have a tractable analytical solution. For the SIS′IS case, treated in the present paper, we use the quasiclassical Andreev equation approach, which, with appropriate modifications, allows the inclusion of electron-impurity scattering, reflection from finite-transparency interfaces, and the effect of electron-phonon scattering on the quantized states formed in the S′ layer. This method has an accuracy $\sim(\Delta/E_F)^2 \approx 10^6$ ($E_F$ is the Fermi energy) for typical metals, and is applicable for arbitrary junction transparency and purity, provided $\tau_i E_F \gg 1$ (where $\tau_i$ is the elastic collision time). The quasiclassical Green function technique has definite advantages when averaging over the effects introduced by disorder, and including the elastic scattering and strong coupling effects.

### A. The Andreev equations

In the present paper we consider stationary states of a double barrier junction which we describe in terms of the retarded electron Green function. The approach is based on the notion of smooth quasiclassical trajectories, and remains valid in the presence of phonons or disorder. The scattering of electrons by phonons or impurities is included using a standard approximation for averaging the self-energy. The

Green function approach is also easily generalized to a nonstationary case, e.g., when an external ac field or a finite bias voltage is applied across the junction. The stationary local electron density of states $\mathcal{N}(\varepsilon)$ in the electrodes of an SIS′IS junction is computed from solutions of the quasiclassical Andreev equations[26,28,29] with appropriate boundary conditions at the sharp interface barriers where the quasiclassical approximation is violated.

The spinor wave function $\hat{\Psi}_l(x,s)$, which obeys the Bogoliubov equations,[26,28] is represented as

$$\hat{\Psi}_l(x,s) = \sum_{K_\parallel}^{\infty} [\hat{\psi}_+(x,K_\parallel)e^{ik_{\mathrm{F}x}x} + \hat{\psi}_-(x,K_\parallel)e^{-ik_{\mathrm{F}x}x}]e^{iK_\parallel s}, \quad (1)$$

where the subscript $l=1,2$ corresponds to two independent solutions of the Bogoliubov equation [one is generated by an electron wave incident from the left ($l=1$) and another one ($l=2$) is generated by a hole wave coming from the right], $s$ is the $(y,z)$ coordinate of the quasiparticle, $K_\parallel$ is $(y,z)$-component of the Fermi momentum, and $k_{\mathrm{F}x} = \sqrt{2mE_{\mathrm{F}} - K_\parallel^2}$ is the $x$ component of Fermi momentum. The slowly varying spinor amplitude $\hat{\psi}_\alpha$ is written

$$\hat{\psi}_\alpha = \begin{pmatrix} u_\alpha \\ v_\alpha \end{pmatrix}, \quad (2)$$

with components $u_\alpha$ and $v_\alpha$ denoting electron and hole *envelope* wave functions on classical trajectories; positive and negative directions are denoted by the index $\alpha = \pm 1$. The spinor $\hat{\psi}_\alpha$ obeys the Andreev equation

$$\hat{\mathcal{H}}_{0\alpha}\hat{\psi}_\alpha = E_\alpha \hat{\psi}_\alpha \quad (3)$$

with

$$\hat{\mathcal{H}}_{0\alpha} = -i\hbar\alpha\hat{\sigma}_3\mathbf{v}_{\mathrm{F}}\cdot\boldsymbol{\nabla} + \mathbf{v}_{\mathrm{F}}\cdot\mathbf{p}_{\mathrm{s}} + \hat{\sigma}_1\Delta e^{i\varphi}; \quad (4)$$

here $\hat{\sigma}_i$ $(i=1,\ldots,3)$ are the Pauli spin matrices, $\mathbf{v}_{\mathrm{F}}$ is the velocity at a point $\mathbf{p}_{\mathrm{F}}$ on the Fermi surface, $\mathbf{p}_{\mathrm{s}}$ is the superfluid momentum, $\varphi$ is the phase of the superconducting order parameter, and $\Delta$ satisfies a self-consistency equation. The quasiclassical equation (3) with the Hamiltonian (4) is obtained under the assumption

$$\hbar v_{\mathrm{F}} q \ll E_{\mathrm{F}}, \quad (5)$$

where $q$ is the envelope wave vector which characterizes "slow" variations of the physical quantities along $x$ (typically $q \sim \pi/\xi_{\mathrm{S}}$, where $\xi_{\mathrm{S}}$ is the BCS coherence length in S). The relation (5) is the definition of quasiclassical motion.[30] The spinor function $\hat{\psi}$ in Eq. (4) constitutes the slowly varying (provided $|\varepsilon| \ll E_{\mathrm{F}}$) envelope of the stationary state wave function. The term $\mathbf{v}_{\mathrm{F}}\cdot\boldsymbol{\nabla}$ in Eq. (4) results in wave packet spreading along the classical trajectory and couples the wave function only on straight lines in the direction of the velocity $\mathbf{v}_{\mathrm{F}}$.

The boundary conditions at a sharp interface are obtained under an assumption that the barrier thickness is comparable to an atomic size; therefore the Andreev amplitudes $\hat{\psi}_\alpha(x,K_\parallel)$ can be regarded as constants in the vicinity of the barrier. The reflection and transmission probabilities are determined by the rapidly oscillating parts $\propto e^{\pm ik_{\mathrm{F}x}x + iK_\parallel s}$. Then, using the fact that the wave functions (1) outside the scattering region are given by a linear combination of the asymptotic solutions, one obtains the boundary conditions at the interface barriers.

## III. A MODEL FOR ANDREEV BOUND STATES IN A SINIS JUNCTION

A *self-consistent* solution of Eq. (3) can only be obtained numerically.[20] However, it is instructive to solve Eq. (3) analytically for a piecewise model for the spatial behavior of $\Delta(x)$ given by

$$\Delta(x) = \begin{cases} 0, & -d/2 < x < d/2, \\ \Delta, & x < -d/2 \text{ or } x > d/2; \end{cases} \quad (6)$$

note we set $\Delta' = 0$ in the S′ layer and thus S′ → N.

Since the insulating barriers I are assumed to have an arbitrary transparency $0 < D < 1$, one must implement special boundary conditions to match the wave functions across the interfaces (i.e., at $x=-d/2$ and $x=d/2$).

In the quasiclassical scenario, particles move between the interfaces along trajectories (shown schematically in Fig. 1(b)); in a clean system these are straight lines characterized by the direction $\mathbf{n}$ of velocity (and some initial position $\mathbf{R}$). At any point in real space, an infinite number of trajectories with different $\mathbf{n}$ cross each other. Between interfaces, such crossings do not lead to observable physical effects, since there are no intertrajectory transitions.

The local electron density of states and the electric current are expressed via the quasiclassical retarded Green function $\hat{g}^R(x)$ which satisfies a causality condition (see Refs. 26 and 28). $\hat{g}^R(x)$ is then constructed from two solutions of Eq. (3), $\hat{\psi}^{l,r}_\alpha(x)$, where $\alpha = \pm 1$ is the direction index mentioned above; the solution $\hat{\psi}^l(x)$ vanishes at $x=+\infty$, while $\hat{\psi}^r(x)$ vanishes at $x=-\infty$. The trial wave functions in directions "±" on a quasiclassical trajectory in the left (L) S electrode ($x < -d/2$) in notation of Ref. 26 are then

$$\hat{\psi}^l_{+L} = \begin{pmatrix} J_L e^{i\varphi_1/2} \\ 0 \end{pmatrix} e^{iqx} + A^l_L \begin{pmatrix} a_1 e^{i\varphi_1/2} \\ e^{-i\varphi_1/2} \end{pmatrix} e^{iqx},$$

$$\hat{\psi}^l_{-L} = B^l_L \begin{pmatrix} b_1 e^{-i\varphi_1/2} \\ e^{i\varphi_1/2} \end{pmatrix} e^{-iqx}, \quad (7)$$

where the primes denote reflected wave amplitudes, $q = \xi_\varepsilon/(v_{\mathrm{F}}\cos\eta)$, $v_{\mathrm{F}} = |\mathbf{v}_{\mathrm{F}}|$, $\eta$ is the angle between $\mathbf{n}$ and the interface normal, $\xi_\varepsilon = \sqrt{\varepsilon^2 - \Delta^2}$, and $\varepsilon$ is the energy variable. The wave $\hat{\psi}^l_\alpha(x)$ is generated by an electron incident from the left $(x=-\infty)$ with $v^l(x)=0$ and $u^l(x) = J_L e^{i\varphi_1/2} e^{iqx}$; here $J_L = \sqrt{1-|a_1|^2}$, and $a$ and $b$ are the elementary amplitudes of Andreev reflection which converts an electron to a hole and a vice versa. The phase difference across the first (second) interface is denoted as $\varphi_{1(2)}$ and the phases have opposite signs for electrons and holes.

The trial wave functions in the N layer $(-d/2 < x < d/2)$ have the form

$$\hat{\psi}^l_{+N} = \begin{pmatrix} D^l_N \\ A^l_N \end{pmatrix} e^{ikx}, \quad \hat{\psi}^l_{-N} = \begin{pmatrix} B^l_N \\ C^l_N \end{pmatrix} e^{-ikx}, \tag{8}$$

where $k=\varepsilon/(v_{\mathrm{F}}\cos\eta)$ and for simplicity we assume that $\eta$ is the same in S and N. $A^l_N$ in Eq. (8) describes the Andreev reflection[29] of an electron from the first interface (incident from the right) as a hole (or equivalently the hole transmission coefficient from L to N), $D^l_N$ is the coefficient of conventional electron reflection from the second interface (back into the N layer), $B_N$ is the conventional electron reflection coefficient from the first barrier (back into the N layer), and $C^l_N$ is the Andreev reflection coefficient[29] of an electron from the second barrier (incident from the left). In the right (R) S electrode ($x>d/2$) one has

$$\hat{\psi}^l_{+R} = C^l_R \begin{pmatrix} b_{2'} e^{i\varphi_2/2} \\ e^{-i\varphi_2/2} \end{pmatrix} e^{iqx}, \quad \hat{\psi}^l_{-R} = D^l_R \begin{pmatrix} a_2 e^{-i\varphi_2/2} \\ e^{i\varphi_2/2} \end{pmatrix} e^{-iqx}, \tag{9}$$

where $C^l_R$ corresponds to an electron incident on the second interface from the right and Andreev-reflected back as a hole into the right superconducting electrode. We emphasize that the above functions (7)–(9) only contain the slowly varying parts of the full wave function $\hat{\psi}(\mathbf{r},t)$ [i.e., varying on the scale of $\sim\hbar v_F/(\pi\Delta)$] while the fast oscillating factor, $\propto\exp(i\mathbf{p}_F\cdot\mathbf{r}/\hbar)$, has been removed from the description. [It can be shown from the more general Bogoliubov equations that the latter gives a small contribution $\sim(\Delta/E_{\mathrm{F}})^2$.] This implies that we do not consider Breit-Wigner-like resonances.[11,31]

For the sake of simplicity we assume that the reflection/transmission at the SIN and NIS interfaces is specular. A generalization to rough interfaces can be made with a technique suggested in Refs. 26 and 32. Reflection/transmission processes mix together semi-infinite quasiclassical electron and hole trajectories. Each of the trajectories is characterized by a Fermi momentum $\mathbf{p}_{\mathrm{F}}$ and a corresponding velocity $\mathbf{v}_{\mathrm{F}}$. The directions of the velocity $\mathbf{v}_{\mathrm{F}}$ are indicated by arrows [see Fig. 1(b)]. Although the classification of in/out trajectories in accordance with the direction of the Fermi velocity is unique, there is a kind of arbitrariness because the electrons [shown as solid lines in Fig. 1(b)] and holes [shown as dashed lines in Fig. 1(b)] belonging to the same trajectory have *opposite* directions of their velocities. The regions inside of which reflection (transmission) occurs, where the classical trajectories get coupled together, are referred to as "knots" and are indicated as solid circles in Fig. 1(b). At these knots, the quasiclassical condition is violated (because the wave function cannot be partioned into smooth-envelope and fast-oscillating parts). In the general case a particle may leave its original trajectory at a knot and switch to another trajectory moving in a different direction. In the simple case of specular reflection assumed here, the knot mixes just two incoming and two outgoing electron/hole trajectories [as shown in Fig. 1(b)]. We will apply the so-called "unitary" boundary conditions at the knots.[26] At the left barrier (positioned at $x=-d/2$) they are written as

$$\begin{pmatrix} B^l_L b_1 e^{-i\varphi_1/2} e^{iqd/2} \\ D^l_N e^{-ikd/2} \end{pmatrix} = \hat{S}_{\mathrm{L}} \begin{pmatrix} A^l_L a_1 e^{i\varphi_1/2} e^{-iqd/2} + J_L e^{i\varphi_1/2} e^{-iqd/2} \\ B^l_N e^{ikd/2} \end{pmatrix} \tag{10}$$

and

$$\begin{pmatrix} A^l_L e^{-i\varphi_1/2} e^{-iqd/2} \\ C^l_N e^{ikd/2} \end{pmatrix} = \hat{S}^{\dagger}_{\mathrm{L}} \begin{pmatrix} B^l_L e^{i\varphi_1/2} e^{iqd/2} \\ A^l_N e^{-ikd/2} \end{pmatrix} \tag{11}$$

while at the right interface barrier ($x=d/2$) one obtains

$$\begin{pmatrix} B^l_N e^{-ikd/2} \\ C^l_R b_{2'} e^{i\varphi_2/2} e^{iqd/2} \end{pmatrix} = \hat{S}_{\mathrm{R}} \begin{pmatrix} D^l_N e^{ikd/2} \\ D^l_R a_2 e^{-i\varphi_2/2} e^{-iqd/2} \end{pmatrix} \tag{12}$$

and

$$\begin{pmatrix} C^l_N e^{-ikd/2} \\ C^l_R e^{-i\varphi_2/2} e^{iqd/2} \end{pmatrix} = \hat{S}^{\dagger}_{\mathrm{R}} \begin{pmatrix} A^l_N e^{ikd/2} \\ D^l_R e^{i\varphi_2/2} e^{-iqd/2} \end{pmatrix}, \tag{13}$$

where $\hat{S}$ is a $2\times 2$ unitary matrix

$$\hat{S}_{\mathrm{L(R)}} = \begin{pmatrix} r_{\mathrm{L(R)}} & -t_{\mathrm{L(R)}} \\ t^*_{\mathrm{L(R)}} & r^*_{\mathrm{L(R)}} \end{pmatrix}, \tag{14}$$

which couples the quasiclassical trajectories; here $r_{\mathrm{L(R)}}$ and $t_{\mathrm{L(R)}}$ are the electron reflection and transmission amplitudes at the left (right) interface barriers.

The above matrix equations (10)–(13) involve eight linear equations for the eight unknown coefficients: $A^l_L$, $B^l_L$, $A^l_N$, $B^l_N$, $C^l_N$, $D^l_N$, $C^l_R$, and $D^l_R$. An additional eight equations involving a similar set of coefficients, with the superscript $l$ replaced by $r$, determine the solution for the case where an electron and hole are generated by an electron incident from $x=+\infty$ with $v^r(x)=0$ and $u^r(x)=J_R e^{i\varphi_2/2} e^{-iqx}$ where $J_R=\sqrt{1-|a_2|^2}$. These two sets of linear inhomogeneous equations for the unknown coefficients are solved analytically using available computer algebra programs.

General characteristics of the multilayered junctions are conveniently described in terms of retarded Green functions having simple analytical properties. In accordance with the recipes of Refs. 26 and 28, the retarded Green function on the classical trajectory is constructed using two linearly independent solutions $\hat{\psi}_+(x)$ and $\hat{\psi}_-(x)$ of the Andreev equation (3). At this point one should implement a different interpretaion of Eq. (3), treating the energy $E_\alpha$ not as an eigenvalue of (4) but rather as a complex variable $\varepsilon$ off the energy spectrum. According to general mathematics, Eq. (3) with a complex $\varepsilon$ has two solutions, which conform to the boundary conditions[26,28]

$$\hat{\psi}_+(x) \to +\infty,$$

$$\hat{\psi}_-(x) \to -\infty. \tag{15}$$

The above solutions are used as building blocks of the retarded Green function, which is analytical in the upper half-plane of the complex $\varepsilon$. In this way, the boundary conditions (15) actually determine the analytical properties of the retarded Green function. According to Ref. 28 the boundary conditions (15) are satisfied for the spinor function

$$\hat{\psi}^{l,r} = \begin{pmatrix} u_{l,r} \\ v_{l,r} \end{pmatrix} \tag{16}$$

if the sign of the imaginary part of $q$ entering Eqs. (7)–(9) [and also in corresponding expressions for $v^r(x)=0$ and $u^r(x)$] is chosen appropriately. Namely, the waves $\hat{\psi}_{+(-)}$ are obtained from the functions $\hat{\psi}^{l(r)}$ as follows. In order to ensure the boundary conditions (15), the wave vector $q=\xi_\varepsilon/(v_F\cos\theta)$ entering the term $\propto e^{iqx}$ in the function (9) is replaced by $q=\{i\sqrt{\Delta^2-\varepsilon^2}\theta(\Delta-|\varepsilon|)+[\sqrt{\varepsilon^2-\Delta^2}\mathrm{sign}(\varepsilon)+i\delta]\theta(|\varepsilon|-\Delta)\}/(v_F\cos\eta)$ (where $\delta\to 0$), while in the term $\propto e^{-iqx}$ it is replaced by $q=\{-i\sqrt{\Delta^2-\varepsilon^2}\theta(\Delta-|\varepsilon|)+[\sqrt{\varepsilon^2-\Delta^2}\mathrm{sign}(\varepsilon)-i\delta]\theta(|\varepsilon|-\Delta)\}/(v_F\cos\eta)$. Similar replacements are also made in other terms entering $\hat{\psi}^{l,r}$. Then the retarded electron matrix Green function can be expressed as follows:

$$\hat{g}^R(x) = \frac{1}{u_l\bar{v}_r + u_r\bar{v}_l}\begin{pmatrix} u_l\bar{v}_r + u_r\bar{v}_l & -u_l\bar{u}_r - u_r\bar{u}_l \\ v_l\bar{v}_r + v_r\bar{v}_l & -u_r\bar{v}_l - u_l\bar{v}_r \end{pmatrix}, \tag{17}$$

where $u_{l,r}$ and $v_{l,r}$ are the spinor components entering (16) and $\bar{v}$ corresponds to an electron with its momentum reversed. Solving Eqs. (10)–(13) for the coefficients of $\hat{\psi}^{l,r}(x)$ and using Eq. (17) along with the expressions for the elementary Andreev reflection amplitudes $a(\varepsilon)=i\Delta/(\varepsilon-\xi_\varepsilon)$ and $b(\varepsilon)=i(\varepsilon+\xi_\varepsilon)/\Delta$, one obtains the quasiclassical Green function. The formula simplifies when the left and right barriers are identical. At $x=-d/2+\zeta$ (where $\zeta$ is infinitesimally small), $\varphi_1=0$, and $\varphi_2=0$, one then obtains

$$G_N(\varepsilon) = [\hat{g}_N^R]_{11} = \frac{\Delta\xi_\varepsilon + r\xi_\varepsilon^2 + r\xi_\varepsilon(\Delta-\varepsilon) + 2r\xi_\varepsilon(\varepsilon-\xi_\varepsilon)e^{i\chi_\varepsilon} + \xi_\varepsilon e^{2i\chi_\varepsilon}(\varepsilon-\xi_\varepsilon)}{r\xi_\varepsilon(\varepsilon-\Delta) + \xi(\varepsilon-\xi_\varepsilon)e^{2i\chi_\varepsilon} - \Delta\xi_\varepsilon - r\xi_\varepsilon^2}, \tag{18}$$

where $\chi_\varepsilon=(\varepsilon d)/(v_F\cos\eta)+\varphi/2$ (where $\eta$ again is the electron incidence angle and we use units with $\hbar=1$). In the limit $r=0$ (which corresponds to ideally transparent interfaces, as might be modeled by an SNS junction) one obtains a well-known expression[28] for the retarded Green function in the middle N layer,

$$G_N^0(\varepsilon) = \frac{\varepsilon\cos\chi_\varepsilon + \xi_\varepsilon\sin\chi_\varepsilon}{\xi_\varepsilon\cos\chi_\varepsilon - \varepsilon\sin\chi_\varepsilon}, \tag{19}$$

which has poles when

$$\frac{\xi_\varepsilon}{\varepsilon} = \tan\chi_\varepsilon. \tag{20}$$

From the solutions of (18) and (19) one finds the probabilities $|a|^2$ and $|b|^2$ for Andreev reflection in the normal (N) region (where an electron is converted into a hole at the N/S interface and vise versa). This induces a nonvanishing pair amplitude in the normal N region (which may be interpreted as a proximity effect); however, in the absence of a pairing potential the gap will be zero. From Eq. (19), which is valid for an SNS junction, one can see that for an electron moving slowly in the direction of an NS interface, i.e., one having a relatively large transverse momentum (implying $\eta\simeq\pi/2$), the phase shift $\chi_\varepsilon$ formally diverges. This may be interpreted as a breakdown of the Andreev approximation, as was emphasized in Ref. 3. This divergence does not occur if the barrier transparency in the junction is finite ($1>D>0$). Below we compute the local density of states for the finite transparency barriers taking into account the contributions of electron-hole trajectories at finite incidence angles $\eta\neq 0$.

At zero temperature and in the absence of elastic scattering (if the junction electrodes are ideally "clean"), the quasiclassical equation (3) is simply the well-known Andreev equation.[29] When the scattering of electrons on impurities and phonons is included via the self-energies, the structure of Eq. (3) is not changed, but they are interpreted as building blocks of the Green functions.[26,28]

## IV. DISCUSSION OF RESULTS ON ANDREEV BOUND STATES

The magnitude of $\Delta$ determines the height of the potential well for excitations in our geometry. The wave functions of quasiparticles with energy $\varepsilon<\Delta$ are localized in the vicinity of the N layer,[28] and their energies are quantized in accordance with the solution of Eqs. (10)–(13) and corresponding levels associated with waves incoming from the right. Although finite interface barriers would ordinarily be expected to reduce the fraction of Andreev reflection in favor of ordinary reflection, an overall resonant enhancement results in sharp levels even for low transparencies $D$, which in experiments are typically $D\approx 10^{-4}-10^{-5}$; here $D=|t|^2$ where $t$ is the parameter entering the $S$-matrix [see Eq. (14)]. In this limit the quantized levels become *even sharper* than in the ideally transparent SNS junction. This behavior is consistent with an elementary quantum mechanical model which describes the interaction between two localized states in adjacent quantum wells. When the interaction is strong (which corresponds to high junction transparency $D\approx 1$), the ABS bands $E_n(\varphi)$ are broad. However if the interwell interaction is weak (i.e., for $D\ll 1$), the ABS bands are narrow. For such a reason the peaks in the local electron density of states are much sharper for $D\ll 1$ than for $D\approx 1$ case. In addition, the Cooper pair transfer through a low transparency SIS′ISSISIS junction results from quite severe quantization conditions which establish the *overall* phase-coherent supercurrent between the left and right S electrodes. As the barrier transpar-

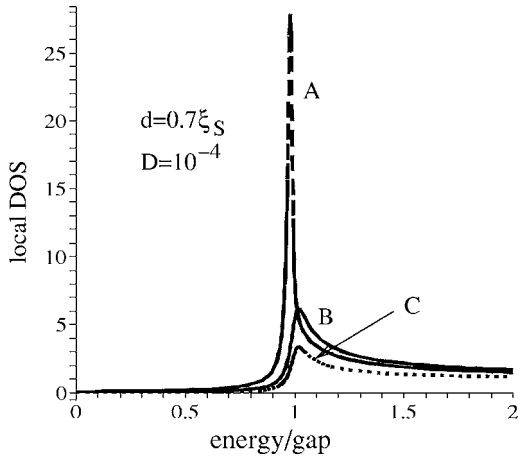


FIG. 2. Curve *A* shows the local density of electron states (DOS) $\mathcal{N}(\varepsilon)$ at the middle of the N layer of a SINIS junction while curve *B* shows the DOS near the junction for the SIS case with the same transparency. Curve *C* shows the DOS of a bulk superconductor.

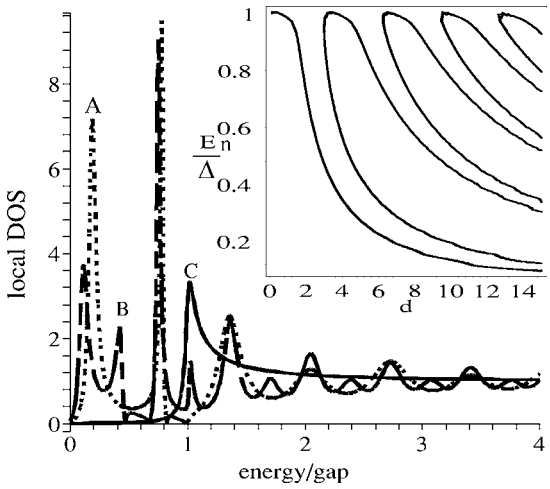


FIG. 3. The local DOS for thicker middle layers (curves *A* and *B*). Curve *C* is the DOS of a bulk superconductor. The inset shows the dependence of the ABS level energy versus *d*, with other parameters of the junction fixed.

ency *D* is lowered, the selection of electrons is stricter: only a small fraction of electrons with definite energy (momentum) are Andreev reflected, while others are reflected conventionally. This strict selection gives a sharp ABS singularity in local electron density of states (DOS), which is mathematically *much stronger* than the BCS singularity $\propto 1/\sqrt{\epsilon-\Delta}$. One can observe this tendency from Fig. 2 where we plot the local electron density of states (DOS), $\mathcal{N}_{\mathrm{N}}(\varepsilon)=\mathrm{Re}\, G_N(\varepsilon)$ [see Eq. (17)], at the center of the N layer of an SINIS junction at $x=-d/2+\zeta$ (where $\zeta$ is infinitesimally small) for $\varphi_1=0$ and $\varphi_2=0$ with $d=0.7\xi_{\mathrm{S}}$ and $D=10^{-4}$. Figure 2 also shows a comparison of the local DOS for an SINIS junction (curve *A*) with the local DOS for an SIS junction (curve *B*, calculated near the SIS interface barrier) having the same combined transparency as the SINIS junction, and the DOS of a bulk superconductor (curve *C*). Note that curve *A* has a very sharp peak at $\varepsilon\simeq\Delta$, while the peaks in curves *B* and *C* are much broader. Such a remarkably sharp peak (as in curve *A*) was experimentally observed in the quasiparticle tunneling conductivity characteristics of SINIS junctions (see Ref. 20). In Fig. 3 we plot the local DOS for $D=10^{-4}$ and for thicker N layers, with $d=4.6\xi_{\mathrm{S}}$ (curve *A*) and $d=9.2\xi_{\mathrm{S}}$ (curve *B*). Curve *C* in Fig. 3 shows the bulk superconductor DOS plotted for comparison. From Fig. 3 one can see that, despite the fact that the junction transparency is quite low ($D=10^{-4}$ in this case), sharp ABS levels occur in the thicker N layer at energies $E<\Delta$. At energies $E>\Delta$ one can see smooth Tomash oscillations (scattering states), the period of which depends on the N layer thickness *d*. The inset in Fig. 3 shows the dependence of the ABS level position versus *d* fixing other parameters of the junction as in the main part of Fig. 3. From this latter plot one can see that the spectral weight of this ABS gradually decreases, and additional levels are created, as *d* increases. Shown in Fig. 3, results are well compatible with earlier results of Ref. 12 where self-consistent calculations of the local DOS were conducted with an exact method based on the Bogoliubov equations.

The above description is readily generalized to include elastic scattering of electrons from impurity atoms and inelastic scattering of electrons from phonons by adding to $\hat{H}_0$ [see Eq. (4)] the appropriate self-energy terms. In Fig. 4 we illustrate the effect of elastic electron-impurity scattering on the ABS level width. In this figure we plot the local DOS in the N layer for three SINIS junctions having the same thickness $d=0.7\xi_{\mathrm{S}}$, but different concentrations of impurity atoms, each characterized by its own electron-impurity scattering time $\tau_i$. All three curves (*A*, *B*, and *C*) have a peak at an energy $E_0\simeq\Delta$; however the peak width strongly depends on $\tau_i$. In particular, if the N layer is relatively clean (i.e., if the strength of the electron-impurity scattering in N is weak, as, e.g., for curve *A* corresponding to $\Delta\tau_i=7.5$), the peak is rather sharp. However, the peak becomes much wider when the electron-impurity scattering becomes stronger (see curves *B* and *C* for which $\Delta\tau_i=1.5$ and $\Delta\tau_i=0.5$). In the "clean" limit, the electron motion is ballistic between the interfaces; thus only a few classical trajectories contribute to the quan-

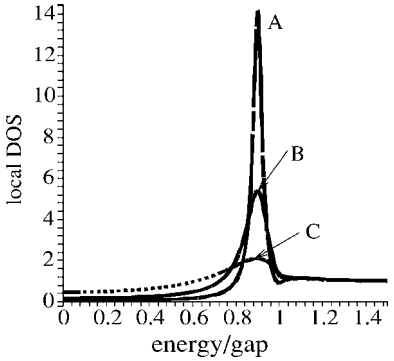


FIG. 4. The influence of elastic electron-impurity scattering on the ABS level width as manifested in the local DOS curves in the N layer for three SINIS junctions having the same thickness as in Fig. 2 but a different concentration of impurity atoms, each characterized by its own electron-impurity scattering time $\tau_i$.

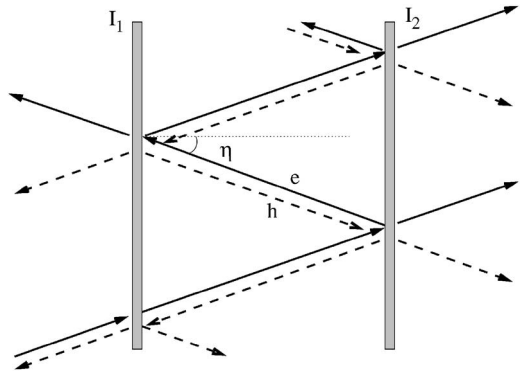


FIG. 5. The network of quasiclassical trajectories which contribute to the broadening of the ABS singularity due to finite-angle reflection/transmission from the interface barriers.

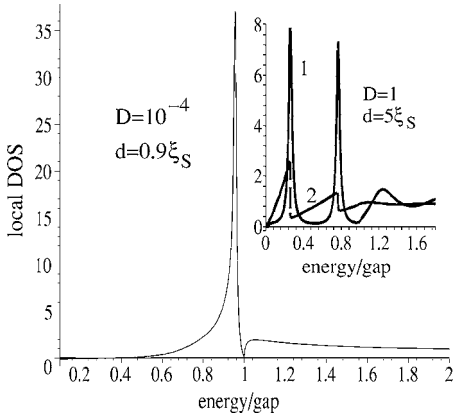


FIG. 6. The angle averaged local DOS in the middle layer of a low transparency SINIS junction. The inset shows the local DOS in an ideally transparent junction; curve 1 is the local DOS for incidence angle $\eta=0$ while curve 2 is the angle averaged DOS.

tization conditions. This gives sharp resonances in the local electron density of states $N_\varepsilon$, which indeed strongly affect the scattering probabilities of elementary processes. In the opposite "dirty" limit, the electron-impurity scattering is strong and the electrons move along complicated trajectories before they are reflected/transmitted through the junction interface. The ABS quantization conditions must then be formulated for each of the classical trajectories separately, but because the length of each trajectory differs, the quantization conditions are different for each trajectory. Since the number of trajectories is large, and the calculated results must be averaged over the all trajectories, the ABS peaks are broadened in the "dirty" limit.

### A. Finite-angle electron-hole trajectories

The numerical results presented above were limited to the case of electrons incident normal to the interface. The inclusion of electrons incident at other angles causes a broadening in the density of states, in addition to that arising from the effects of scattering. The pieces of quasiclassical trajectories between two consequent knots are then longer than in the case of normal incidence (see Fig. 5 where solid lines correspond to electrons and the dash lines to holes). This modifies the resonance condition, shifting the ABS level associated with that electron-hole pair down in energy. From Fig. 5 one can infer that the finite angle processes ($\eta \neq 0$) yield a quite complicated network of quasiclassical trajectories. To treat this case we must implement a numerical approach for solving the boundary conditions. The result obtained depends on the interface barrier transparency. When the interface transparency is ideal ($D=1$), the ABS peaks are greatly broadened when the contribution of finite-angle processes is included. In the inset to Fig. 6 we plot the calculated results for double-barrier junctions with $D=1$ and $d=5\xi_S$. Curve 1 in Fig. 6 with two sharp ABS peaks at $\varepsilon=0.25\Delta$ and $\varepsilon=0.75\Delta$ is the local DOS in the middle layer ($x=0$) when the incidence angle $\eta=0$. However, the angle-averaged local DOS given by curve 2 has much lower "saw tooth" maxima at the same energies. This broadening of the angle-averaged peaks is caused by the contribution of the finite-angle reflection/transmission processes which substantially reduce the resonant properties of multilayered ideally transparent junctions. The situation is quite different when the junction transparency is low, $D \ll 1$. Assuming a specular character of transmission/reflection at the interface barrier we find that the finite-angle contribution is not significant and the sharp ABS peaks persist in the angle-averaged local DOS. Using the quasiclassical trajectories network shown in Fig. 5, and utilizing the fact that the electron transmission amplitude $t$ at a finite incidence angle $\eta \neq 0$ acquires an additional finite-angle barrier factor $\propto \exp[1-1/(v_F \cos\eta)]$, we computed the angle-averaged local DOS numerically. A typical angle-averaged local DOS is plotted in Fig. 6 for $D=10^{-4}$ and $d=0.9\xi_S$. We emphasize that the finite-angle barrier factor $\propto \exp[1-1/(v_F \cos\eta)]$ eliminates the processes with $\eta \simeq \pi/2$ which violated the quasiclassical approximation in the case $D=1$. One can see a remarkably sharp peak at $\varepsilon=0.95\Delta$ corresponding to the ABS singularity and a smooth shoulder just below $0.95\Delta$ arising from the the finite-angle processes. Physically, the reason why the finite-angle reflection/transmission processes are not significant is because the low-transparency interface barriers serve as "filters," which favor strictly resonant processes (e.g., with $\eta=0$), while weaker processes (e.g., with $\eta \neq 0$) average out. The electrons and holes with normal incidence therefore give the dominant contribution to the physical properties of the double-barrier junctions, while the finite-angle processes are less significant. The transverse size of the junction is assumed as being much larger comparing to the BCS coherence length in S and smaller than the Josephson penetration depth. A single sharp ABS is well pronounced for low transparent junctions ($D \leqslant 10^{-4}$) even if the transverse size $L_t$ is substantial, $L_t \gg \xi_S$. In this case satellite peaks coming from finite-angle trajectories are very weak and wide.

### B. Spatial extent of ABS states

The Andreev bound states have several inherent features which make them unique among quantized states in other systems. One remarkable property is that the ABSs are not strictly localized inside the potential well formed by a mini-

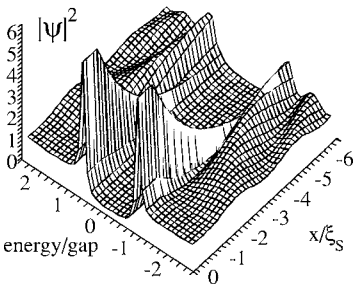


FIG. 7. The probability density function $|\hat{\psi}(x)|^2$ versus the electron energy and spatial coordinate $x$ (in units of the coherence length.)

mum of the superconducting gap $\Delta(x)$, as happens, e.g., for Breit-Wigner resonant states. Instead, the ABSs penetrate the adjacent superconducting electrodes over a much larger distance than the BCS coherence length, $\xi_{\mathrm{BCS}}$. This property can be described in terms of the Andreev equations (3) and (4) with the trial wave function (7)–(9) with the term $J_L e^{i\varphi_1/2}$ omitted. Using the quasiclassical boundary conditions one obtains eight homogeneous linear equations that are completed by the normalization condition

$$\int_{-\infty}^{\infty} |\hat{\psi}(x)|^2 dx = 1$$

from which we obtain the energy-dependent coefficients $A_L$, $B_L$, $A_N$, $B_N$, $C_N$, $D_N$, $C_R$, and $D_R$. The probability density function $|\hat{\psi}(x)|^2$ is plotted in Fig. 7 for $\varepsilon=0.3\Delta$ and $d=0.9\xi_{\mathrm{S}}$ assuming $D=0.9$.

## V. ELECTRON-PHONON RECOMBINATION RATE FROM AN ABS LEVEL

As is shown in Fig. 1(a), the Cooper pair transfer mechanism across the double-barrier junction involves the ABS levels. If the superfluid current is time dependent (which is the case when an external dc or ac field is applied), its properties depend not only on the level height and width but also on the characteristic lifetime during which the elementary excitations reside in the level. The lifetime $\tau_{\mathrm{ABS}}=(\nu_\varepsilon^{\mathrm{e\text{-}p}}+\nu_\varepsilon^{\mathrm{e\text{-}e}})^{-1}$ is governed by the inelastic collision rates, $\nu_\varepsilon^{\mathrm{e\text{-}p}}$ and $\nu_\varepsilon^{\mathrm{e\text{-}e}}$, of an electron with phonons and with other electrons in the system. Since the collisions cause an eventual recombination of the Cooper pairs and electrons to a steady state, the rates $\nu_\varepsilon^{\mathrm{e\text{-}p}}$ and $\nu_\varepsilon^{\mathrm{e\text{-}e}}$ serve as useful microscopic characteristics of the multilayered junction. When the temperature $T$ is low ($T\ll\Delta$, which is the case of interest for many experiments and practical applications) the electron-phonon recombination processes dominate over the electron-electron contribution ($\nu_\varepsilon^{\mathrm{e\text{-}p}}\ll\nu_\varepsilon^{\mathrm{e\text{-}e}}$), and the latter can be neglected. The function $\nu_\varepsilon^{\mathrm{e\text{-}p}}$ then determines the low-temperature dynamics of multilayered junctions. In this subsection we implement the Keldysh method[33] to compute the electron-phonon recombination rate $\nu_\varepsilon^{\mathrm{e\text{-}p}}$ using results of the previous subsection. The expression for $\nu_\varepsilon^{\mathrm{e\text{-}p}}$ is given by[33]

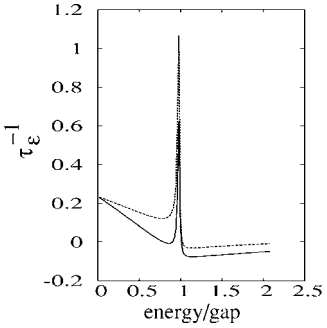


FIG. 8. The dependence of the electron-phonon recombination rate $\nu_\varepsilon^{e\text{-}p}$ versus electron energy $\varepsilon$ for two different temperatures, $T=\Delta/5$ (curve $A$) and $T=\Delta/8$ (curve $B$).

$$\nu_\varepsilon^{\mathrm{e\text{-}p}}=\frac{\pi\lambda}{4(sp_{\mathrm{F}})}\int_0^\infty \omega^2 d\omega(\varpi_+ + \varpi_- + \varpi_1), \tag{21}$$

where $\lambda$ is the electron-phonon coupling constant, $s$ is the sound velocity, $p_{\mathrm{F}}$ is the Fermi momentum,

$$\varpi_+ = \theta([\varepsilon+\omega]^2-\Delta^2)L_{\varepsilon,\varepsilon+\omega}(N_\omega+n_{\varepsilon+\omega}),$$

$$\varpi_- = \theta([\varepsilon-\omega]^2-\Delta^2)L_{\varepsilon,\varepsilon-\omega}(n_{\varepsilon-\omega}-N_\omega-1),$$

$$\varpi_1 = -L_{\varepsilon,\omega-\varepsilon}(N_\omega+n_{\omega-\varepsilon}), \tag{22}$$

where $L_{\varepsilon_1,\varepsilon_2}=\mathcal{N}(\varepsilon_1)\mathcal{N}(\varepsilon_2)-\mathcal{M}(\varepsilon_1)\mathcal{M}(\varepsilon_2)$. The local electron density of states $\mathcal{N}(\varepsilon)$ in the middle electrode of an SINIS junction entering Eqs. (21) and (22) was calculated in Sec. IV, while the Cooper pair amplitude $\mathcal{M}(\varepsilon)$ is obtained in a similar way. The electron $n_\varepsilon$ and phonon $N_\omega$ distribution functions entering Eqs. (21) and (22) must in general be obtained from corresponding kinetic equations. However, if the deviation from equilibrium is small, a reasonable evaluation of $\nu_\varepsilon^{\mathrm{e\text{-}p}}$ is obtained by substituting into Eqs. (21) and (22), the equilibrium Fermi and Bose distribution functions. The numerically computed dependence of the electron-phonon recombination rate $\nu_\varepsilon^{\mathrm{e\text{-}p}}$ versus $\varepsilon$ is plotted in Fig. 8 for two different temperatures, $T=\Delta/5$ (curve $A$) and $T=\Delta/8$ (curve $B$). From these curves one can see that $\nu_\varepsilon^{\mathrm{e\text{-}p}}$ vanishes at $\varepsilon\simeq\Delta$ which corresponds to the ABS energy $E_0$. That means that the electron-phonon recombination time, $\tau_{\mathrm{e\text{-}p}}(\varepsilon)=1/\nu_\varepsilon^{\mathrm{e\text{-}p}}$, diverges at the ABS level. Our numerical calculations show a similar behavior for the electron-electron recombination time, $\tau_{\mathrm{e\text{-}e}}(\varepsilon)=1/\nu_\varepsilon^{\mathrm{e\text{-}e}}$, which also diverges at the same energy $E_0$. These results demonstrate that the low-temperature dynamics of multilayered junctions with ABS can be remarkably different from the dynamics of conventional Josephson junctions.

## VI. CONCLUSION

The quasiclassical model implemented in this paper gives a tractable description of the quantized ABSs in multilayered Josephson junctions. Using this model, the local electron density of states in the middle layer of an SIS′IS junction versus the interface barrier transparency, and the middle

layer thickness and purity, has been computed. The general trend that follows from the analysis is that sharp ABS levels are formed in a low-transparency SIS′IS junction ($D \leqslant 10^{-4}$) with a "clean" middle layer (with a thickness comparable to or less than the superconducting coherence length, i.e., $d \leqslant \xi_S$), when the electron transport across the layer is ballistic. For an SINIS junction with a wider middle layer ($d \gg \xi_S$), additional ABSs with energies $E_n < \Delta$ are formed. In the opposite limit of a thin middle layer (i.e., when $d \ll \xi_S$) the ABSs exist as well, but the resonances are much weaker and levels are much broader than for the intermediate case $d \leqslant \xi_S$. The elastic scattering of electrons by nonmagnetic impurity atoms in the middle S′ (or N) electrode weakens the ABS resonances, particularly when $\Delta \tau_i \ll 1$. In a low-transparency limit the local electron density of states (DOS) has a resonant character which results in sharp peaks at the ABS level positions. The main contribution to local DOS comes from Andreev reflection processes involving electrons and holes incident perpendicular to the barriers, while the processes with a finite incidence angle are less significant. Unlike quantized states in normal systems, the ABS are not strongly localized in the quantum well, and their spatial extent can be much wider than the width of the well. Another distinguished feature is that the inelastic electron-phonon recombination time, $\tau_{e\text{-}p}(\varepsilon)$, associated with an ABS level $E_0$ is a sharp function of energy variable $\varepsilon$ and diverges at $\varepsilon = E_0$, which is not the case for a normal system. The results obtained in this paper are well consistent with recent experiment[20] where the current-voltage ($I$-$V$) characteristics of SIS′IS junctions were measured. The vertical step in the $I$-$V$ curve observed in Ref. 20 at the bias voltage $V = \Delta/e$ was interpreted as the injection of Cooper pairs into the ABS level, while the sharp peak in the tunneling conductivity at $V \approx 2\Delta/e$ was attributed to the quasiparticle injection into the same level. The experimentally observed features are much stronger (by the factor ~10 in Ref. 20 and by the factor ~100 in more recent experiments) than it was expected from the multiple Andreev reflection (MAR) processes[22–24] but can be understood when using the present model. We conclude that the superconducting junctions with ABS energy bands have a number of remarkable properties which may be useful in various experimental and technical applications.

## ACKNOWLEDGMENT

This work was supported by the National Science Foundation under Grant No. EIA-0218652.

*Also at Institute of Magnetism NASU, 36b Vernadsky Blvd., 03142 Kyïv, Ukraine.
†URL: http://pubweb.northwestern.edu/~ssh192
‡Also at Materials Research Center and the Department of Electrical and Computer Engineering, Northwestern University, Evanston, Illinois 60208.

[1] J. Bardeen, R. Kümmel, A. E. Jacobs, and L. Tewordt, Phys. Rev. **187**, 556 (1969).
[2] O. Kulik, Zh. Eksp. Teor. Fiz. **57**, 1745 (1969) [Sov. Phys. JETP **30**, 944 (1970)]; C. Ishii, Prog. Theor. Phys. (Kyoto) **44**, 1525 (1970).
[3] R Kümmel, Phys. Rev. B **10**, 2812 (1974).
[4] G. B. Arnold, Phys. Rev. B **18**, 1076 (1978); G. B. Arnold, J. Low Temp. Phys. **68**, 1 (1987).
[5] G. Kieselmann, Phys. Rev. B **35**, 6762 (1986).
[6] Y. Tanaka and M. Tsukada, Phys. Rev. B **44**, 7578 (1991).
[7] A. Furusaki and M. Tsukada, Phys. Rev. B **43**, 10164 (1991); C. W. J. Beenakker and H. van Houten, Phys. Rev. Lett. **66**, 3056 (1991).
[8] L.-F. Chang and P. F. Bagwell, Phys. Rev. B **49**, 15853 (1994).
[9] S. E. Shafranjuk and T. Yamashita, Phys. Rev. B **54**, 15380 (1996).
[10] I. P. Nevirkovets and S. E. Shafranjuk, Phys. Rev. B **59**, 1311 (1999).
[11] A. Brinkman and A. A. Golubov, Phys. Rev. B **61**, 11297 (2000).
[12] C. Ciuhu, A. Lodder, R. E. S. Otadoy, and R. T. W. Koperdraad, J. Phys.: Condens. Matter **15**, 1847 (2003).
[13] R. E. S. Otadoy and A. Lodder, Phys. Rev. B **65**, 024521 (2001).
[14] P. Miller and J. K. Freericks, J. Phys.: Condens. Matter **13**, 3213 (2001).
[15] J. K. Freericks, B. K. Nikolic, and P. Miller, Phys. Rev. B **64**, 054511 (2001); Erratum: **68**, 099901(E) (2003).
[16] H. F. Hess, R. B. Robinson, R. C. Dynes, J. M. Valles, Jr., and J. V. Waszczak, Phys. Rev. Lett. **62**, 214 (1989); Ch. Renner, A. D. Kent, Ph. Niedermann, Ø. Fischer, and F. Lévy, *ibid.* **67**, 1650 (1991).
[17] Y. Levi, O. Millo, N. D. Rizzo, D. E. Prober, and L. R. Motowidlo, Phys. Rev. B **58**, 15128 (1998).
[18] I. P. Nevirkovets, J. B. Ketterson, and S. Lomatch, Appl. Phys. Lett. **74**, 1624 (1999).
[19] S. E. Shafranjuk, I. P. Nevirkovets, and J. B. Ketterson, Solid State Commun. **121**, 457 (2002).
[20] I. P. Nevirkovets, S. E. Shafranjuk, and J. B. Ketterson, Phys. Rev. B **68**, 024514 (2003).
[21] I. P. Nevirkovets, O. Chernyashevskyy, and J. B. Ketterson (unpublished).
[22] M. Octavio, M. Tinkham, G. E. Blonder, and T. M. Klapwijk, Phys. Rev. B **27**, 6739 (1983).
[23] E. N. Bratus, V. S. Shumeiko, E. V. Bezuglyi, and G. Wendin, Phys. Rev. B **55**, 12666 (1997).
[24] D. Averin and A. Bardas, Phys. Rev. Lett. **75**, 1831 (1995).
[25] E. Scheer, W. Belzig, Y. Naveh, M. H. Devoret, D. Esteve, and C. Urbina, Phys. Rev. Lett. **86**, 284 (2001).
[26] A. Shelankov and M. Ozana, Phys. Rev. B **61**, 7077 (2000).
[27] A. V. Zaitsev, Zh. Eksp. Teor. Fiz. **86**, 1742 (1984) [Sov. Phys. JETP **59**, 1015 (1984)].
[28] A. V. Svidzinsky, *Space-inhomogeneous Issues of the Superconducting Theory* (Science, Moscow, 1982) (in Russian).
[29] A. F. Andreev, Sov. Phys. JETP **19**, 1228 (1964).
[30] N. B. Kopnin, *Theory of Nonequilibrium Superconductivity* (Clarendon Press, Oxford, 2001).
[31] A. V. Galaktionov and A. D. Zaikin, Phys. Rev. B **65**, 184507 (2002).
[32] Y. Nagato and K. Nagai, Phys. Rev. B **69**, 104507 (2004).
[33] L. V. Keldish, Sov. Phys. JETP **20**, 1018 (1965); G. M. Eliashberg, *ibid.* **34**, 668 (1972).